Three-phase metal-insulator transition and structural alternative for a VO2 film epitaxially grown on Al2O3(0001)

Aude Bailly, Stéphane Grenier, Michelle M. Villamayor, Michael Gaudin, Aline Y. Ramos, Pierre Bouvier, Christophe Bouchard, Laurence Magaud, Laetitia Laversenne, Bernard Mongellaz, et al.

Three-phase metal-insulator transition and structural alternative for a VO_2 film epitaxially grown on Al_2O_3(0001)

A. Bailly, S. Grenier, M. M. Villamayor,[a)] M. Gaudin, A. Y. Ramos, P. Bouvier, C. Bouchard, L. Magaud, and L. Laversenne

Univ. Grenoble Alpes, CNRS, Grenoble INP, Institut Néel, 38000 Grenoble, France

B. Mongellaz and E. Bellet-Amalric

Univ. Grenoble Alpes, CEA, CNRS, INAC, MEM, 38000 Grenoble, France

A. Lacoste and A. Bès

Univ. Grenoble Alpes, CNRS, LPSC, 38000 Grenoble, France

(Dated: October 2, 2020)

We report on the crystallographic phases and their epitaxial relationships observed during the metal-insulator transition (MIT) of a VO_2 film deposited on $Al_2O_3(0001)$. A key feature of this work is to establish two possible in-plane epitaxial relationships for the VO_2 film, introducing an *on-axis* and a *diagonal* model. These models have distinctive signatures in reciprocal space in the form of multiplet reflections, and can therefore be easily differentiated by diffraction. They serve as a basis for interpreting the results gained by high resolution X-ray diffraction, and complemented by Raman spectroscopy, on a 420 nm-thick VO_2 film grown by microwave plasma-assisted reactive sputtering on $Al_2O_3(0001)$. We address its orientation and follow its structure through the MIT. The film is oriented according to the *diagonal* model and exhibits a MIT involving three phases with different temperature domains of (co)existence. The room- and high-temperature phases are respectively identified as the monoclinic M1 and rutile R polymorphs of VO_2. Additionally, we observe that when the sample resistivity starts to decrease, the insulating M1 phase turns into an intermediary phase, which then partially transforms into the metallic R phase when the MIT is complete. The intermediary phase is similar to the M2 polymorph of VO_2, according to its lattice parameters, Raman signature and its known proximity with the M1 and R phases in tensile conditions. The mixing of the M2 and R phases is still detected at 110°C, *i.e.* far above the MIT; the M2 polymorph being probably stabilised at the interface between the film and the substrate, where the interfacial strain is higher.

[a)]Also at Univ. Grenoble Alpes, CNRS, LPSC, 38000 Grenoble, France; Current address: Division of Solid State Electronics, The Angström Laboratory, Uppsala University, Box 534, 751 21 Uppsala, Sweden

I. INTRODUCTION

Bulk VO_2 undergoes a first-order metal-insulator transition (MIT) at the critical temperature of $T_{MIT} \sim 68°C$. It switches from a transparent, insulating and monoclinic phase at room temperature (RT) to an opaque, metallic and tetragonal rutile-like phase above T_{MIT}.[1] This archetypal strongly-correlated electron material has triggered an intense field of research from a fundamental point of view[2,3] and as a potential component in devices[4] like optical filters,[5] memory materials,[6,7] passive radiators[8] or thermochromic windows.[9] However, most of these applications require to adapt the MIT features (transition temperature, hysteresis width and amplitude) to the optical and/or electrical properties required in the conditions of use. The characteristics of the MIT are mainly correlated to the variation of the V-V distances along the c_R axis of the rutile structure and the modification of the vanadium valence state. This is usually achieved by doping VO_2 with a chemical impurity[10] or by inducing a strain along the c_R axis.[11] This latter approach can be realized by growing epitaxial VO_2 films on selected substrates, like TiO_2 and Al_2O_3 single crystals, leading to highly-oriented films of good crystalline quality. As such, strain engineering offers a wealth of possibilities for tailoring the films' properties and has therefore motivated a great number of studies over the past years. It relies on the control of the c_R axis length by generating a compressive or a tensile strain along the corresponding direction. The dependence of the transition temperature T_{MIT} on the length of the c_R axis was suggested.[12] A shorter c_R length (associated to shorter V^{4+}-V^{4+} distances) is expected to induce a decrease of T_{MIT}, even down to RT. A compressive strain along the c_R direction would result in an overlapping of the *d* orbitals, therefore stabilising the rutile metallic phase. The effect of the interfacial strain on the transition temperature was also illustrated for VO_2 films of different thicknesses grown by oxide molecular beam epitaxy (MBE) on $TiO_2(001)$; the transition temperature shifting to higher temperature as the thickness increases.[13] In the case of (0001)-oriented Al_2O_3 (also known as c-cut sapphire), resistivity ratios of more than four orders of magnitude have been achieved (for films generally thicker than 100 nm)

using various growth techniques, such as Pulsed Laser Deposition (PLD),[14] electron-beam deposition,[15] MBE[16] and sputtering.[17] The synthesis conditions turn out to play a major role on the MIT characteristics, not only through the specific deposition parameters (principally, the substrate temperature and the oxygen partial pressure), but also through the growth kinetics. This sensitivity towards the synthesis conditions arises from the complex V-O phase diagram.[18] The importance of the difference in thermal expansion coefficients between VO_2 and the chosen substrate was therefore stressed,[19] as well as the role of possible defects, such as oxygen vacancies.[20,21] An additional intricacy arises from the existence of several VO_2 polymorphs with close free energies. The most frequently reported crystal structures are the tetragonal rutile R phase (space group: $P4_2/mnm$) above T_{MIT}, and the monoclinic M1 polymorph ($P2_1/c$) at RT. The latter exhibits a dimerization of the V atoms aligned in a twisted arrangement along the c_R axis of its parent tetragonal structure. It was also observed that the MIT from M1 to R might involve other polymorphs of VO_2, depending on external pressure or lattice strains.[22] Additional metastable phases have thus been reported, such as the monoclinic M2,[23] the A $(P4_2/nmc)$ and B $(C2/m)$ phases,[24,25] as well as a triclinic T $(C\bar{1})$ polymorph. In the M2 phase ($C2/m$), half of the V atoms are arranged similarly to the M1 polymorph, and the other half are paired in strictly linear chains along the tetragonal c_R axis.

These aspects all together explain why several epitaxial relationships have been observed for a given sapphire orientation. For instance, Azhan *et al.* reported on the synthesis of micrometer-sized crystallites of $(011)_{M1}$-oriented VO_2 on $Al_2O_3(0001)$ using reactive sputtering,[26] whereas changing the substrate bias led to smaller crystallites exhibiting a $(010)_{M1}$-oriented growth. It was also shown that $(010)_{M1}$-oriented VO_2 films grown on $Al_2O_3(0001)$ following two PLD procedures can adopt two distinct in-plane epitaxial relationships, leading to quite different transport properties.[27] The in-plane angular difference between the two orientations was small (only a few degrees), but led to peculiar signature in reciprocal space: the $(220)_{M1}$ X-ray reflection showed a dou-

blet structure for the sample grown at RT and subsequently annealed, whereas a triplet structure was observed for the sample grown directly at 500°C.

In this work, we introduce two structural models (called hereafter *on-axis* and *diagonal*) to account for the possible epitaxial relationships of a $[010]_{M1}$-oriented VO_2 film on $Al_2O_3(0001)$. We then report on the structural study of a 420 nm-thick VO_2 film grown by microwave plasma-assisted reactive sputtering[28] on such a substrate, by combining High-Resolution X-Ray Diffraction (HRXRD) and Raman spectroscopy. HRXRD provides clear evidence that the growth proceeds according to the *diagonal* model. At RT, the monoclinic structure is similar to the M1 bulk phase. When raising the temperature above 66°C, this phase entirely transforms into an intermediary phase similar to the M2 polymorph. Further increase of the temperature leads to the appearance of a slightly distorted rutile R phase at the expense of the intermediary phase. The transformation is not complete; the intermediary phase persisting until at least 40°C above the phase transition temperature.

	Space group	a (Å)	b (Å)	c (Å)	β or γ (°)	V (Å^3)	Ref.
M1	$P2_1/c$	5.752	4.538	5.382	122.65	118.29	[29]
M2	$C2/m$	9.083	5.763	4.532	91.3	2×118.58	[30]
R	$P4_2/mnm$	4.554	4.554	2.856	90	0.5×118.44	[31]
Al_2O_3	$R\bar{3}c$	4.759	4.759	12.993	120		[32]

Table I. Bulk lattice parameters of Al_2O_3 and of a selection of VO_2 published phases: monoclinic M1 and M2 (25°C) and tetragonal rutile R (127°C).

II. TWO POSSIBLE IN-PLANE EPITAXIAL ORIENTATIONS

Before reporting on our findings, we first would like to clarify some inaccuracies we discuss later about the epitaxial relationship of a VO_2 film deposited on a $Al_2O_3(0001)$ substrate. Our XRD results indicate that the high temperature (HT) rutile VO_2 poly-

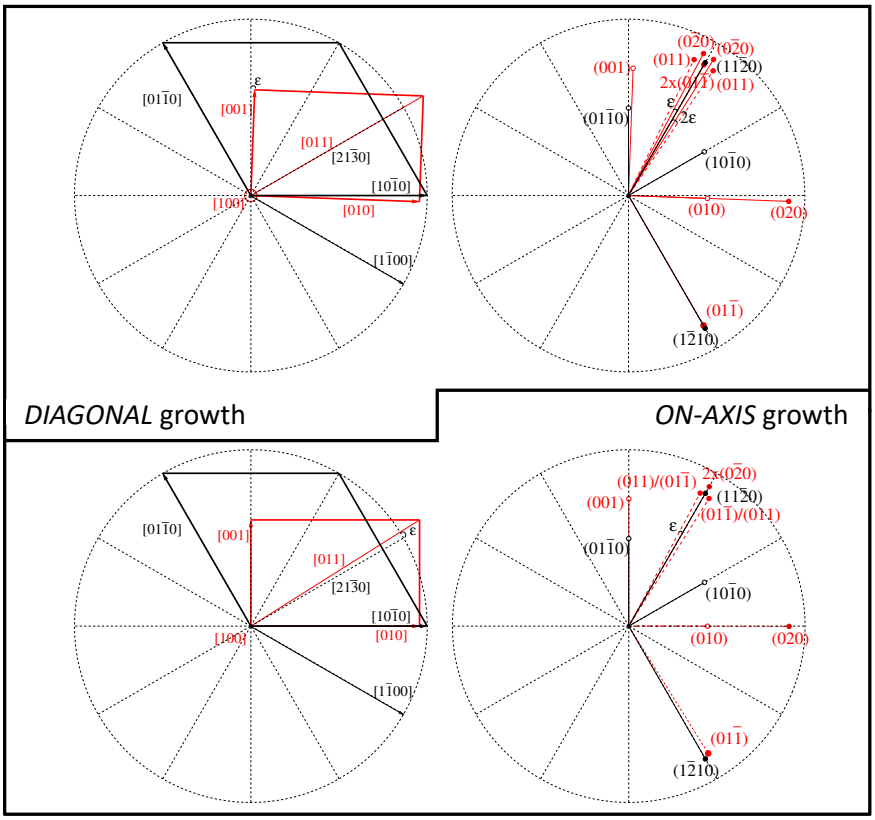

Figure 1. Representations of the two growth models for a thick $[100]_R$-oriented VO_2 film deposited on $Al_2O_3(0001)$: *diagonal* (top) and *on-axis* (bottom). In each case, the left (right) schematic represents the direct (reciprocal) space. In direct space, the black surface unit-cell corresponds to the Al_2O_3 substrate and the red one, to the rutile R polymorph of VO_2. ε corresponds to the angular shift between the two surface unit-cells. In reciprocal space, blank (filled) circles indicate forbidden (allowed) reflections and dashed lines mark 30° rotations. The symmetry operations leading to the observations of the triplet, doublet and singlet structures by diffraction are described in the text ("2×(*hkl*)" indicates the superposition of two such reflections arising from two domains). Not all reflections are represented, except around the substrate's $(11\bar{2}0)$ one.

morph grows with its $\overrightarrow{a}$ axis perpendicular to the substrate's surface; the out-of-plane epitaxial relationship is therefore $[100]_R \parallel [0001]_{Al_2O_3}$. As to the in-plane relationship, we have drawn two models that explain our experimental results and most of those from the literature. In the following, the (*hkl*) reflections of the VO_2 polymorphs and the (*hkil*) ones of the sapphire substrate are assigned according to the structures of which bulk lattice parameters are reported in Table I.

The two models are sketched in Figure 1. They have in common the growth direction, but differ by the in-plane epitaxial relationships adopted by the VO_2 film on the sapphire substrate, aligning either on the $[10\bar{1}0]_{Al_2O_3}$ or on the $[21\bar{3}0]_{Al_2O_3}$ directions:

- in the *diagonal* model: $[011]_R \parallel [21\bar{3}0]_{Al_2O_3}$,
- in the *on-axis* model: $[010]_R \parallel [10\bar{1}0]_{Al_2O_3}$ and $[001]_R \parallel [12\bar{3}0]_{Al_2O_3}$.

These two models are rotated by $\varepsilon = 2.09°$ from each other due to the angle of $32.09°(= 30° + \varepsilon)$ between the $[011]_R$ diagonal direction and the $[010]_R$ axis in the HT tetragonal rutile bulk unit cell. For a matter of clarity, only one $[100]_R$-grown unit-cell of the six rutile domains has been represented (in red) on the $Al_2O_3(0001)$ substrate (in black). For the *diagonal* growth, a second domain corresponds to the $[\bar{1}00]_R$-grown domain of which diagonal is aligned on the $[1\bar{1}00]_{Al_2O_3}$ direction. The four other domains are built by a $\pm 120°$ rotation implied by the symmetry of the Al_2O_3 surface.

The corresponding partial (*hk*0) reciprocal spaces are shown in the right-hand part of Figure 1. The (020), (011) and $(01\bar{1})$ reflections from one rutile domain are represented, together with the equivalent reflections from the five other twin domains. The equivalent reflections from the six domains appear either aligned, or shifted by $\pm\varepsilon$ or $\pm 2\varepsilon$ from the substrate's reflections. For the *diagonal* model, the $(011)_R$ reflection from one domain lies -2ε off the $(11\bar{2}0)_{Al_2O_3}$, whereas the $(01\bar{1})_R$ reflection from the domain rotated by +120° from the first one, is aligned with the $(11\bar{2}0)_{Al_2O_3}$ reflection, and so on for the 4 other domains, leading to doublets or triplets (Fig. 1, top right). For an equidistribution of domains under the beam footprint, the central peak of the triplets is expected to be

twice as intense as the two others. Moreover, its Bragg angle is the same than the one of the two other components at high temperature, but not at room temperature as the reflections are not equivalent anymore. Instead, the *on-axis* model exhibits only doublets and singlets (Figure 1, bottom right), respectively for the (011) and the (020) reflections and their equivalents. Therefore these two growth orientations can be very easily disentangled thanks to the multiplet structure of their diffraction patterns.

III. EXPERIMENTAL DETAILS

The 420 nm-thick VO_2 film was grown by plasma-assisted reactive sputtering on a c-cut sapphire substrate, kept at 500°C during deposition. A stationary plasma of an Ar/O_2 mixture (3.4% O_2) at very low pressure (0.27 Pa) was obtained using the multi-dipolar microwave plasma technology powered with 2 kW (evenly distributed on 20 dipolar microwave couplers)[33]. Three pure (> 99.95 at. %) V targets were positioned on a multi-target holder[28] placed on top of the plasma chamber at 12 cm from the substrate. The plasma production (plasma potential $V_p \sim 20$ V) is entirely decoupled from the biasing of the targets and the substrate. The latter was kept at a floating potential ($\sim$ 8 V), while the targets were negatively polarized by applying a 600 V pulsed DC bias. For a 5 Hz pulse frequency, the VO_2 stoichiometry has been achieved by a correlative adjustment of the duty-cycle (50%) and deposition time (4 h).

Figure 2 (top) shows images of the VO_2 film microstructure with increasing magnification, obtained by Scanning Electron Microscopy (SEM). The VO_2 film is composed by large elongated grains with smaller grains in between. Figure 2 (bottom) shows the evolution of the resistivity measured by the 4-point probe technique, while cycling the sample between RT and 98°C under He atmosphere. The metal-insulator transition is correlated to an abrupt resistivity change over more than four orders of magnitude. The minimum of the first-order derivative on the heating (cooling) step peaks at 69°C (63.7°C). The hysteresis is therefore very sharp ($\Delta T \sim 5$°C).

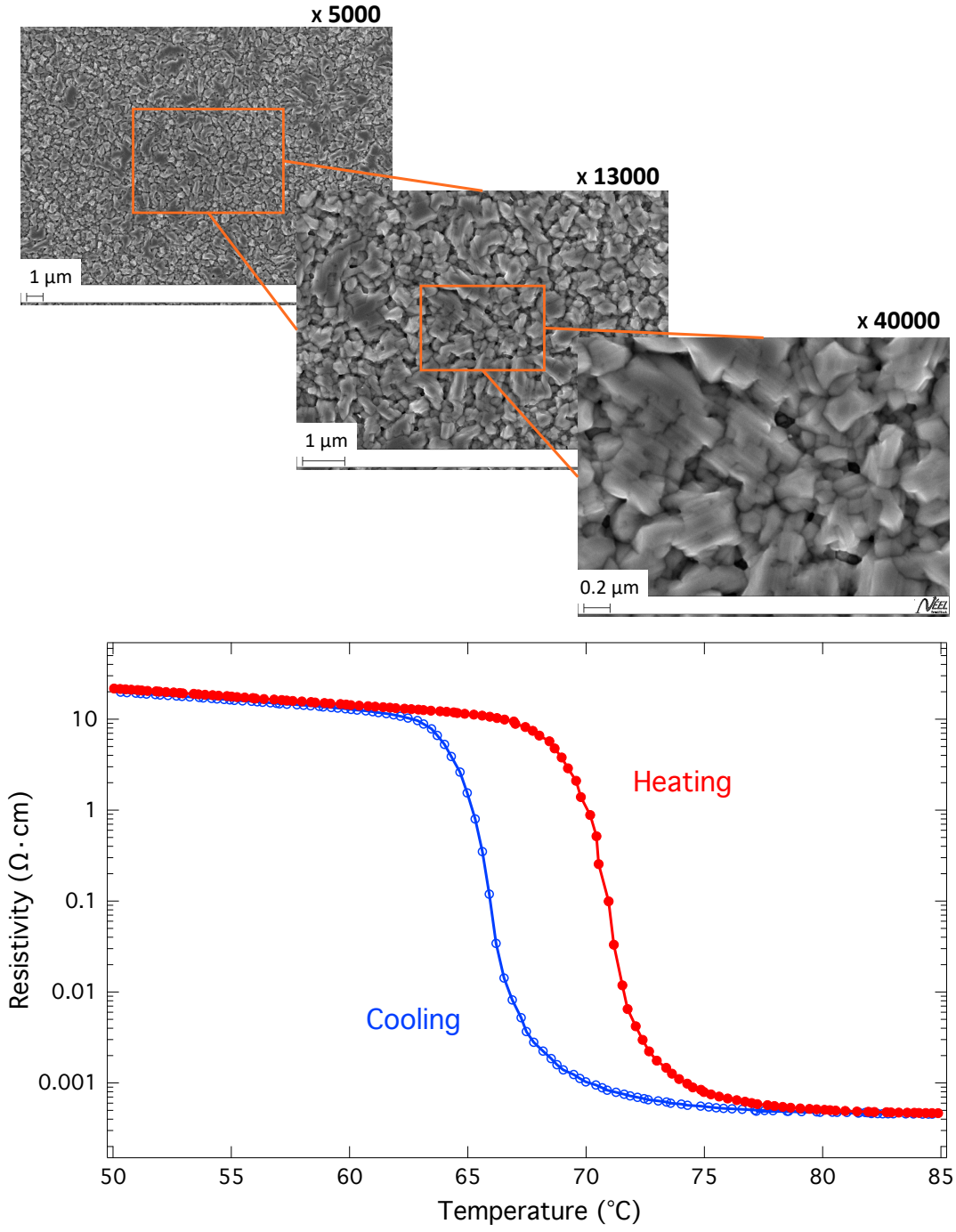

Figure 2. (Top) SEM images of the 420 nm-thick VO_2 film at different magnifications. (Bottom) Close-up on the resistivity measured during a complete temperature cycle (heating and then cooling between RT and 98°C).

X-ray set-up The high resolution X-ray measurements were performed on a SmartLab X-ray diffractometer (Rigaku Corp.) consisting of a 9 kW rotating Cu anode and a 5-circle goniometer. The temperature-dependent X-ray measurements have been performed from RT up to 90°C. The sample temperature was controlled with a precision of ± 1°C using an Anton Paar oven, capped with a carbon dome and maintained in a nitrogen atmosphere to avoid sample oxidation upon heating. The alignment of the sample surface with respect to the incident beam, as well as of the reflections, was systematically conducted at each temperature to counteract extrinsic thermal effects. The X-ray beam footprint was of several mm^2. Depth sensitivity arises from the X-ray penetration length into the material, which correlates with the incidence angle. The critical angle α_c for total external reflection is close to 0.3° at Cu K_α energy (0.35° for VO_2 and 0.29° for Al_2O_3). The crystalline phases present in the film thickness were identified using the out-of-plane scattering geometry, meaning the scattering vector has one component perpendicular to the surface. More specifically, classical $\theta/2\theta$ specular scans were performed. The out-of-plane scattering configuration also includes $\omega/2\theta$ scans of asymmetrical reflections (lattice planes inclined with respect to the sample surface). In these two cases, the incident X-ray beam was monochromatised with a 2-bounce Ge(220) crystal (λ = 1.5405 Å for Cu Kα_1). The whole VO_2 film thickness is probed when performing an asymmetrical or a specular scan (incidence angle of several degrees implying a probed depth of a few micrometers). The in-plane epitaxial relationships of the VO_2 film with respect to the sapphire substrate were determined using a specific configuration that probes the lattice planes perpendicular to the sample surface. In this case, the scattering vector is parallel to the film surface. The X-ray beam impinges the sample in grazing incidence and an additional degree of freedom allows to move the detector in the in-plane direction. The Ge monochromator was removed for these measurements in order to increase the count rate. In such acquisitions, only a few tens of nanometers of the film are probed (incidence angle equal to 0.5° or less).

Raman set-up Unpolarized Raman scattering experiments have been performed in

a backscattering geometry with a Horiba T64000 spectrometer using only one 1800 grooves.mm^{-1} grating and rejecting the Rayleigh line with a laser-flat beamsplitter (LP02-514RE-25 RazorEdge Dichroic, Semrock) in order to measure a relative wavenumber range of 100 to 750 cm^{-1}. A continuous argon laser beam (λ = 514.5 nm) was focused into a spot of $\sim$ 1 μm in diameter on the VO_2 film surface using a long-distance objective ($\times$40 magnification). The laser power was adjusted to 0.25 mW after the objective in order to have enough signal and avoid any thermal effect that could induce a transition to the high-temperature rutile phase. A temperature-controlled stage (Linkam, THMS 600 controller) was used for heating and cooling the sample in a temperature range between 30°C and $\sim$100°C. It was swept by an argon flux in order to avoid a transformation towards a higher oxidation state of VO_2, such as V_2O_5 or V_6O_{13} often observed when heated in air.[34]

IV. GROWTH ORIENTATION AND IN-PLANE EPITAXIAL RELATIONSHIPS

VO_2 growth direction Specular diffraction measurements at RT (Fig. 3) show the sapphire (0006) and (00012) reflections and two other peaks identified as the $(020)_{M1}$ and $(040)_{M1}$ reflections of the VO_2 film. A faint signal due to the $(004)_{M1}$ reflection is also detected at $2\theta \sim 86.3°$, on the high angle side of the $(040)_{M1}$ reflection (see Fig. 7). The $[010]_{M1}$ VO_2 growth orientation on c-cut sapphire is further confirmed with the asymmetric $(022)_{M1}$ and $(110)_{M1}$ reflections shown in Figure 4. This out-of-plane orientation was already reported in several works on VO_2 films grown on $Al_2O_3(0001)$.[22,35–38] It implies a $[100]_R$ growth direction according to the structural transformation linking the M1 and R bulk structures.[31]

In-plane orientations In the following, ϕ corresponds to the sample azimuth, *i.e.* the angle of rotation around the sample normal direction. The ϕ-scan of the asymmetrical $(11\bar{2}6)$ substrate reflection exhibits the 60° hexagonal periodicity of the $\{11\bar{2}6\}$ family

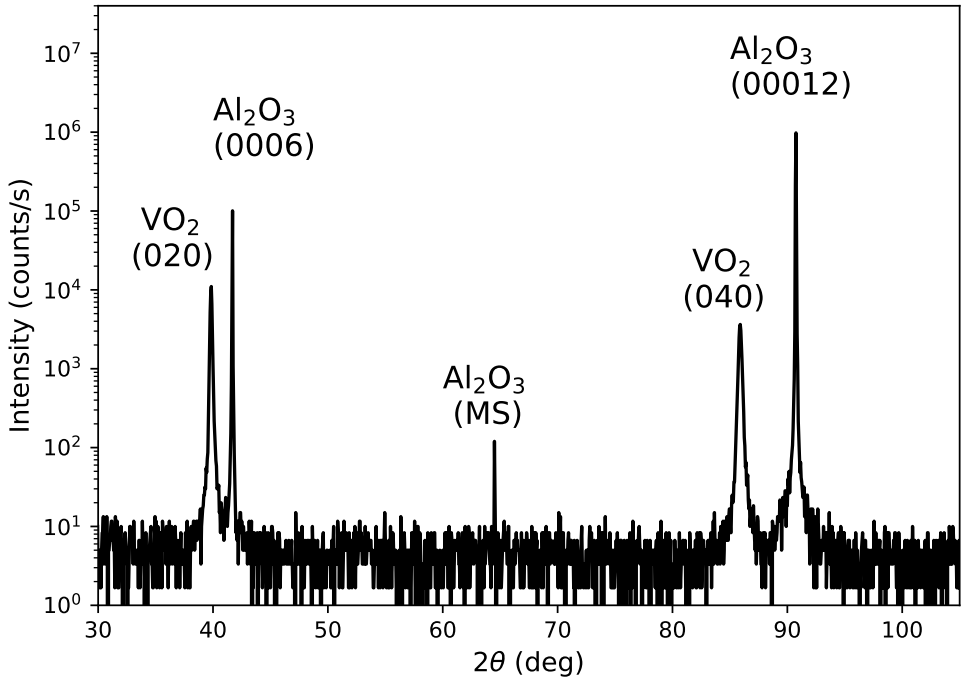

Figure 3. Specular $\theta/2\theta$ scan of the 420 nm-thick VO_2 film at room temperature. The reflections associated to the VO_2 film correspond to the M1 polymorph. MS stands for multiple scattering.

(Fig. 4, top). The VO_2 $(022)_{M1}$ and $(110)_{M1}$ equivalent reflections are found with the same periodicity. They appeared respectively as doublets and triplets; each group being symmetrically centred on the reflections of the substrate. We checked several $(hkl)_{M1}$ reflections of the VO_2 film at RT and all of them presented either a doublet for $h = 0$ (reflections $(022)_{M1}$, $(012)_{M1}$ and $(014)_{M1}$), or a triplet structure for $h \neq 0$ (reflections $(110)_{M1}$, $(230)_{M1}$, $(\bar{2}22)_{M1}$ and $(\bar{2}10)_{M1}$).

In-plane reflections were recorded at grazing incidence in order to increase the sensitivity to the VO_2 film and to be able to detect potential variations of the crystallographic structure with depth. Figure 4 (bottom) shows the grazing-incidence reciprocal space maps (GIRSM) close to the $(11\bar{2}0)$ reflection of the substrate, at room temperature (left)

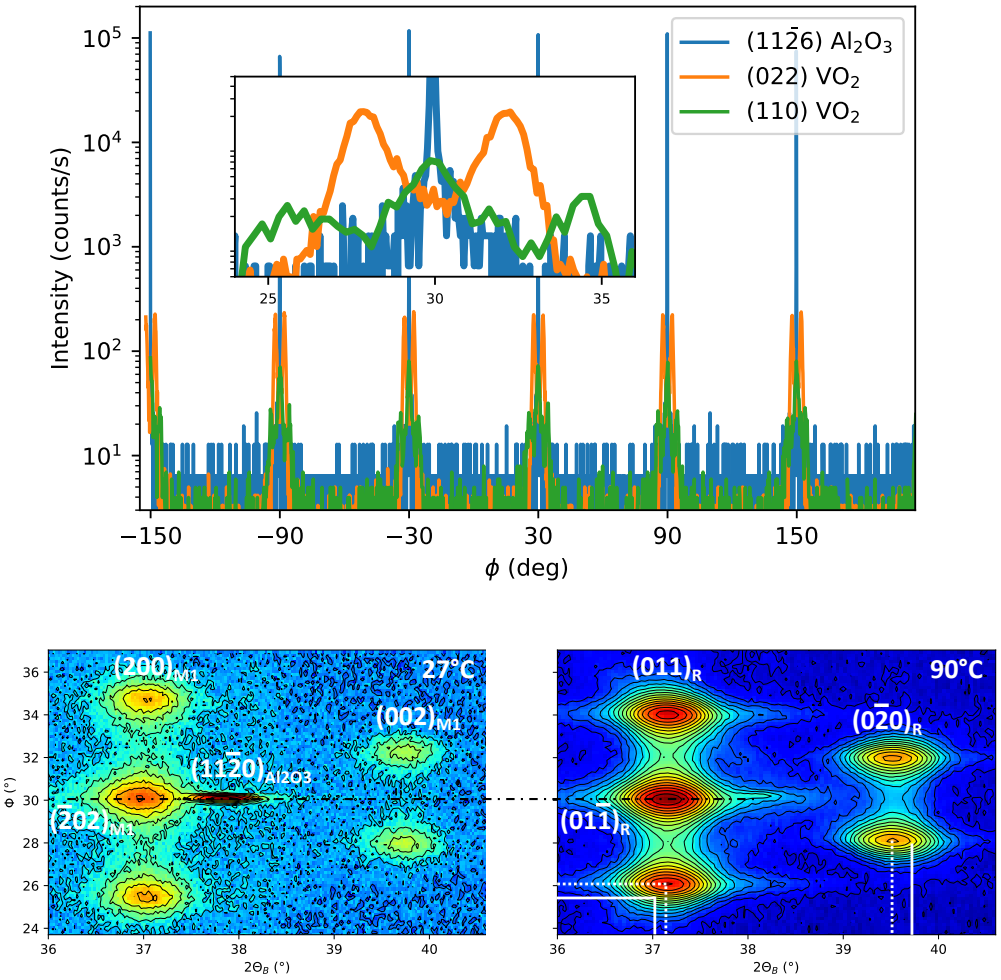

Figure 4. (Top) Room temperature azimuthal scans through the Al_2O_3 $\{11\bar{2}6\}$ reflection family and the VO_2 $(022)_{M1}$ and $(110)_{M1}$ equivalent reflections, appearing respectively as doublets and triplets centred on the reflections of the substrate. The inset is a zoom on the data near $\phi = 30°$. (Bottom) In-plane GIRSM in the vicinity of the $Al_2O_3(11\bar{2}0)$ reflection recorded below and above the MIT (left: at 27°C; right: at 90°C), with the triplet and doublet features of the VO_2 reflection families (indexing corresponds to the *diagonal* model's reciprocal space represented in Fig. 1). Plain (dashed) lines indicate the position of the peaks at 27°C (90°C) to underline the angular shifts induced by the phase transition.

and at 90°C (right). The incidence angle ω was set to 0.5° for the RT map and to 0.2° at 90°C. The lower incidence angle chosen in this latter case emphasizes the signal coming from the VO_2 film at the expense of the substrate's one; thereby extinguishing the $(11\bar{2}0)_{Al2O3}$ reflection (maximum of intensity for $\omega \sim 1°$). We found the distinctive triplet and doublet reflections, peaking respectively at $2\theta_B = 36.9°$ (37.2°) and $2\theta_B = 39.75°$ (39.55°) at RT (90°C). The intensity ratio of the components within the triplet is 1/2/1 (see Fig. 4). As explained above, all these reflections come from six different types of domains. The triplets can be assigned to two superposed $(\bar{2}02)_{M1}$ equivalent reflections at $\phi = 30°$, and two $(200)_{M1}$ equivalent reflections at $\phi = 30 \pm 4.6°$. The doublets correspond to two $(002)_{M1}$ equivalent reflections. At RT, the central peak of the triplet ($(\bar{2}02)_{M1}$ reflection) lies at a slightly lower Bragg angle than the two other equivalent peaks ($(200)_{M1}$ reflection). It follows the same trend as in bulk VO_2. In the HT phase, the triplet is assigned to two $(011)_R$ reflections as satellites and two equivalent $(01\bar{1})_R$ reflections at the center, perfectly aligned with the $(11\bar{2}0)_{Al2O3}$ reflection of the substrate. The doublet corresponds to two $(0\bar{2}0)_R$ reflections. All these observations definitely point to a growth proceeding according to the *diagonal* model.

V. TEMPERATURE-DEPENDENT STRUCTURAL CHANGES

The system was carefully monitored around the MIT temperature using Raman scattering and HRXRD. Both techniques reveal the occurence of a transition involving three phases.

A third phase detected by Raman spectroscopy. The Raman signal is highly sensitive to the point group symmetry. It can thus help to follow the transition and to distinguish the M1 (point group: C_{2h}^3), M2 (C_{2h}^5) and R (D_{4h}^{14}) lattices.[39] The Raman signature of the M1 phase is extensively documented in the literature and is mainly characterized by an intense $A_g(1)$ and $A_g(2)$ doublet at 190 and 225 cm^{-1}, as well as a broad intense $A_g(6)$ peak located around 620 cm^{-1}. This latter is in fact composed by

three distinct peaks:[40–43] a strong one at 618 cm^{-1} and two weak shoulders at 595 and 670 cm^{-1}. The monoclinic M2 phase, less documented, was first examined by Raman spectroscopy in chromium-doped VO_2[44] and its occurence is generally associated to the observation of an intense broad peak at 640 cm^{-1}.[45,46] Similarly to the M1 phase, the M2 one is also characterized by a doublet at low frequency, but with an up-shift of the Ag(1) (at 201 cm^{-1}) and Ag(2) components (at 228 cm^{-1}) compared to the M1 phase. As for the Ag(3) mode, the Raman signature features a downshift from 308 cm^{-1} to 296 cm^{-1} respectively for the M1 and M2 phase.[47–49] The Raman spectrum of the rutile R phase is featureless,[50,51] as a result of the drastic reduction of the Raman intensity due to the metallic character of this phase.

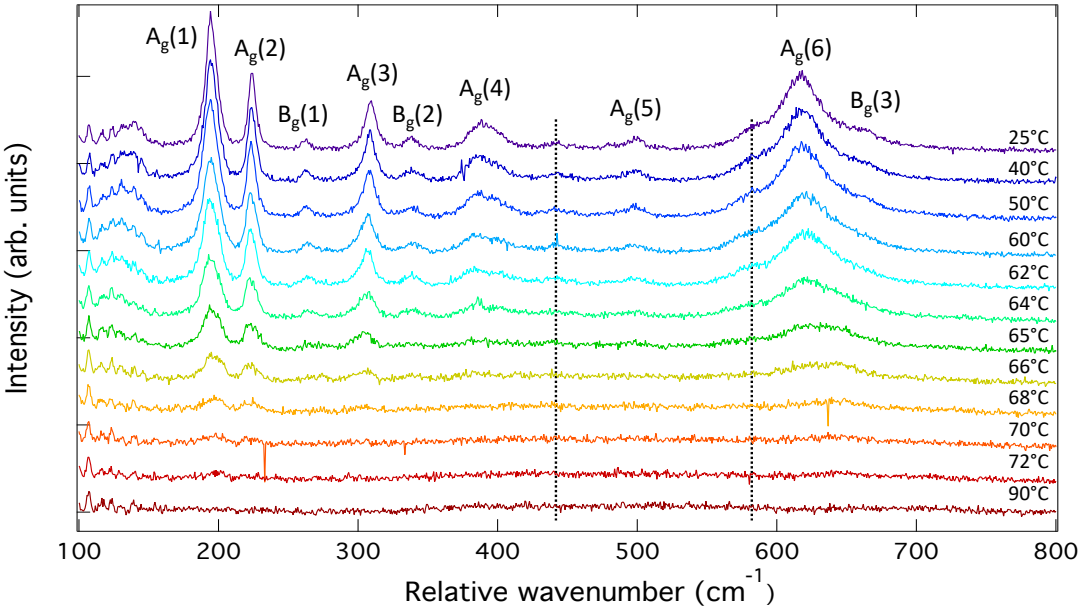

Figure 5. Raman spectra acquired during a cooling step from 90°C down to RT. Peaks at 194, 223, 310, 387, 500 and 617 cm^{-1} are A_g modes of the M1 monoclinic phase of VO_2. The peaks at 261, 339 and 661 cm^{-1} correspond to the B_g ones. Peaks at 441 and 586 cm^{-1} indicated by dashed lines are ascribed to the vibration modes of the c-cut sapphire substrate.

Figure 5 shows a series of Raman spectra collected while cooling down the sample

from 90°C to 25°C. Measurements on warming (not shown) are qualitatively very similar to the ones obtained upon cooling. Above 75°C, the complete absence of the Raman signal indicates that the film consists mainly of the rutile metallic phase. Upon cooling, a broad and faint signal appears at 70°C, becoming maximum and well-resolved at RT. According to the literature, the Raman signature at RT is compatible with the presence of the pure monoclinic M1 phase of VO_2 (A_g modes at 194, 223, 310, 387, 500 and 617 cm^{-1} and B_g modes at 261, 339 and 661 cm^{-1}).

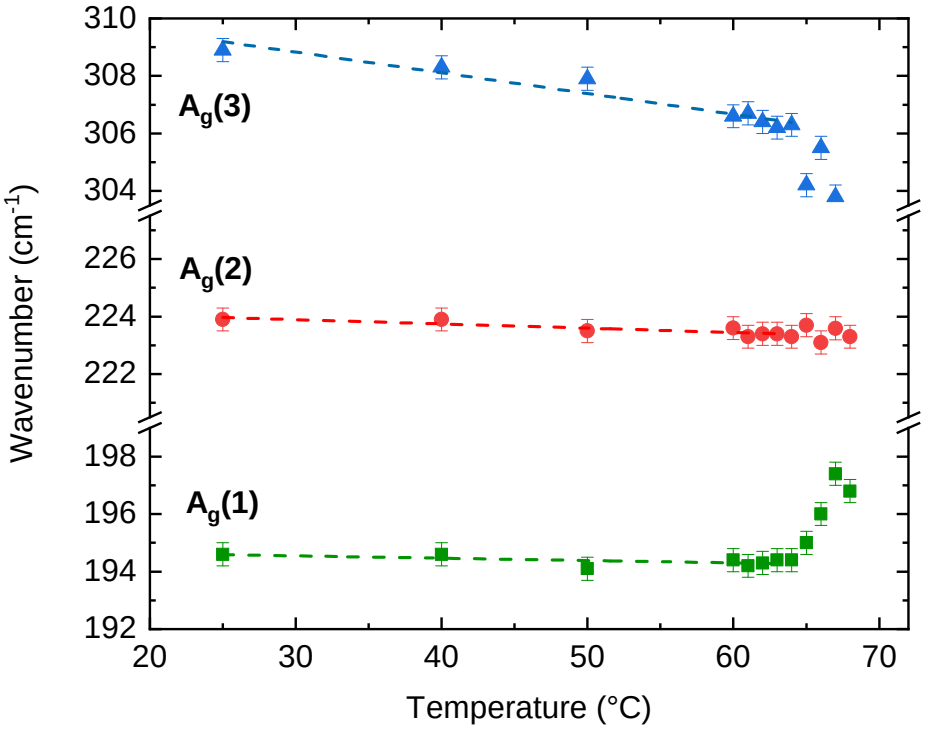

Figure 6. Evolution of the position of the $A_g(1)$, $A_g(2)$ and $A_g(3)$ modes upon cooling. The trend lines between RT and 64°C are displayed as guides for the eyes.

Figure 6 shows the temperature dependence (recorded on cooling) of the wavenumber of the first three A_g phonon modes of the monoclinic phase. For the $A_g(1)$/$A_g(2)$

doublet, it results from the decomposition of the Raman signal between 150 and 250 cm^{-1} with two independent Lorentzian functions and a linear background. In the temperature range between 25°C and 64°C, the expected gradual phonon softening due to lattice thermal expansion with increasing temperature is observed (and materialized with dot lines as a guide for the eyes). For higher temperatures, the behaviour is non monotonous with an upshift for the $A_g(1)$ mode and a downshift for the $A_g(3)$ mode, respectively. No frequency displacement is visible for the $A_g(2)$ mode in our measurements. The high temperature behaviour is assigned to the structural transition from M1 to M2. Actually, the signal broadening due to temperature does not allow to distinguish the specific Raman signatures of M1 and M2 phases. However, the continuous evolution of the Raman signal results from the addition of the two signals and reflects the coexistence of the two monoclinic phases, in particular the appearance and growth of the M2 phase, as expected from the first-order nature of the transition. This was often observed,[45,49,52] but rarely kept as a criterion for the appearance of the M2 phase. Instead, several authors considered the appearance of the high wavenumber $A_g(6)$ peak at 640 cm^{-1} as the indication of the presence of the M2 phase.[45,49,53,54] We also observed (not shown in the figure) a hardening of the $A_g(6)$ mode from 617 to 645 cm^{-1} at 65°C and above. However, as this mode is much broader than the $A_g(1)$ and $A_g(2)$ modes, the determination of the critical temperature where M2 appears is less precise. Thus, the wavenumber evolution of the $A_g(1)$/$A_g(2)$ doublet and the $A_g(3)$ phonon clearly reveals a M1-M2-R phase transformation with increasing temperature.

X-ray study of the transition (specular data). The $(040)_{M1}$ specular reflection was measured while the sample was gradually heated from RT up to 90°C (Fig. 7, top), together with the (00012) reflection of the Al_2O_3 substrate monitored for reference (not shown; shifting from $2\theta_B \sim 90.70°$ to $\sim 90.66°$ due to thermal expansion). From RT up to pre-transition temperature (66°C), the $(040)_{M1}$ reflection can be fitted by a single Voigt component, whose position evolves from $2\theta_B \sim 85.89°$ at RT to 85.86° at 66°C. At this temperature, a second component faintly appears at a lower $2\theta_B$ value (slight

shoulder on the cyan curve). This component keeps on increasing with temperature, while the $(040)_{M1}$ VO_2 Bragg peak progressively vanishes and disappears at 72°C. Surprisingly, from 72°C and above, it is necessary to introduce two distinct components to account for the shape of the reflection peaking at the lowest $2\theta_B$ value. Such a deconvolution was already reported and attributed to the coexistence of two VO_2 phases around the MIT temperature.[22] Our data indicate that two phases are concomitant from 72°C up to at least 90°C. We attribute the component having the intermediate $2\theta_B$ value to the rutile R phase $(400)_R$ Bragg peak. The second component having the lowest $2\theta_B$ value and appearing at T $\sim$ 66°C might correspond to the M2 phase we previously identified by Raman spectroscopy.

For each temperature of the heating cycle, the three components (M1, M2 and R) have been fitted. In the temperature range spanning from 68°C to 74°C, we failed to simultaneously fit the three components: for either the R or the M1 phase, the peaks were too faint to be fitted without strong constraints. The resulting integrated intensities are reported as a function of temperature in Figure 7 (bottom). From RT up to 72°C, the M1 phase gradually disappears, while the M2 phase peak intensity starts to regularly increase from 66°C. At 72°C, the M1 phase has totally disappeared and the R phase is already present. The peak intensity corresponding to the M2 phase is also maximum. Above 72°C, the M2 peak intensity begins to slowly decrease at the benefit of the R phase. Above 78°C, the peaks' intensities barely evolve and stabilize. Given the known unit-cell transformations, the M2 phase would be [100]-oriented, meaning that the specular reflection recorded here is the $(800)_{M2}$.

X-ray study of the transition (GIRSM data). GIRS maps (Fig. 4) are snapshots of the VO_2 film in-plane structure below and above the MIT temperature. In order to gain a detailed understanding of the crystallographic evolution with temperature, we recorded the in-plane doublet and triplet features during a complete heating step. The doublets and triplets behave in a similar way with respect to temperature and therefore, only the triplets are considered hereafter. The mean angular deviation $\Delta\phi$ between the

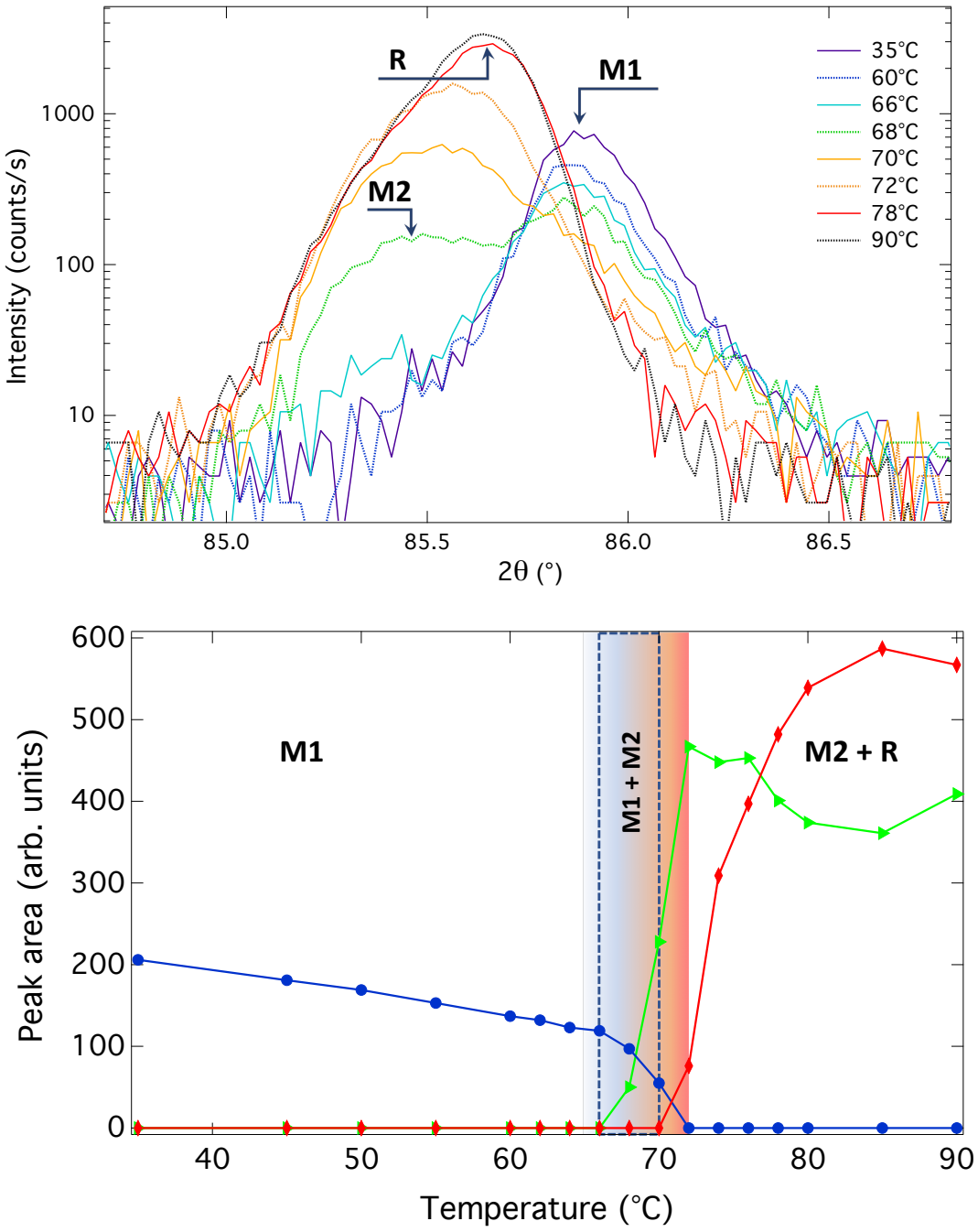

Figure 7. (Top) Evolution of the $(040)_{M1}$ specular reflection of the VO_2 film as a function of the temperature during a heating step. Note that at low temperature, the reflection is asymmetric: the faint component at $2\theta \sim 86.3°$ is assigned to the $(004)_{M1}$ reflection of $[001]_{M1}$-oriented domains. (Bottom) Temperature-dependent existence of the three VO_2 phases evidenced during a heating step, as measured by the peak integrated areas determined from the evolution of the specular reflection intensity (presented above). The color code is as follows: M1 in blue, M2 in green and R in red.

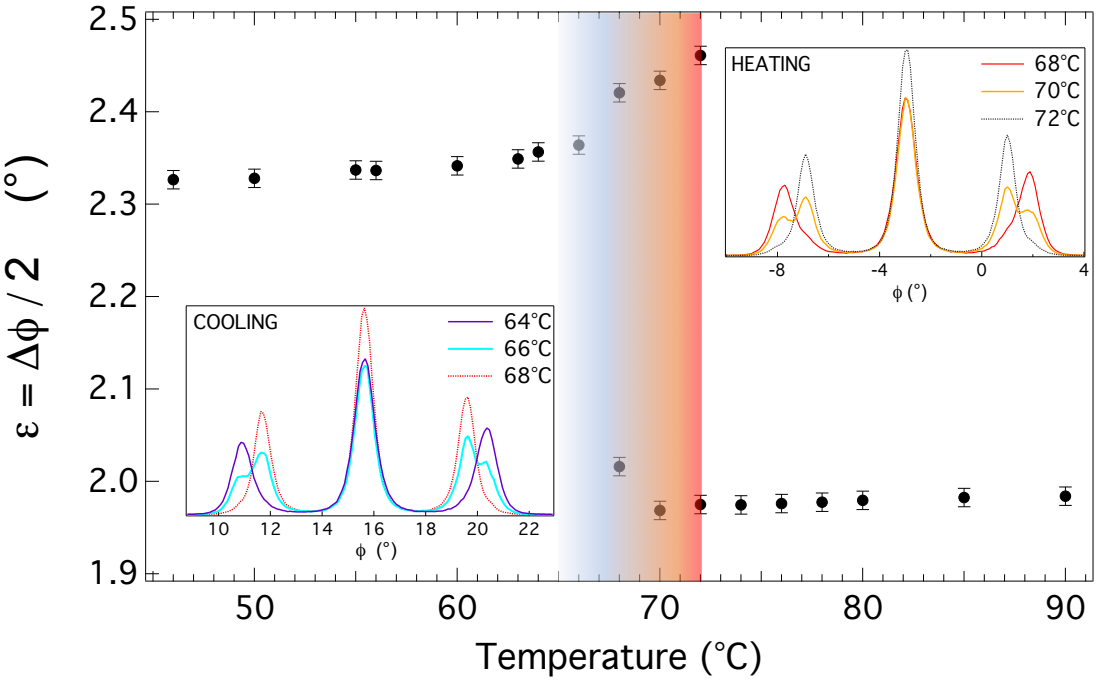

Figure 8. Evolution of the ε value of the triplet upon a temperature increase from RT up to 90°C. ε corresponds to half of the angular separation $\Delta\phi$ between two neighbouring peaks of the triplet. Insets: profiles of the triplets at selected temperatures around the MIT, on heating (upper right corner) and cooling (lower left corner). Below and above the hysteresis temperature range indicated by the color filling, the profiles are quasi-identical. See Figure 4 for the indexing of the reflections at RT and at high temperature.

lateral components of the triplet and the central peak has been determined at every temperature. In the *diagonal* model, it corresponds to $\Delta\phi = 2\varepsilon$. Its variation with temperature is shown in Figure 8. The insets show the evolution of a triplet close to the transition temperature. The data reveal subtle variations of ε. Up to ~ 65°C, ε is close to 2.32°. It then increases very slightly to more than 2.4° in the region of the MIT and finally drops down to less than 2° for temperatures higher than 70°C. The temperature domain, in which ε increases, corresponds to the range where a mixture of M1 and M2 phases was highlighted by the X-ray specular data (Fig. 7).

The lattice parameters derived from our HRXRD measurements are listed in Table II.

	a (Å)	b (Å)	c (Å)	β or γ (°)	V (Å^3)	T (°C)
M1	5.742	4.523	5.353	122.15	117.7	46
M2	9.083	5.777	4.535	(91.3)	2×118.95	68
R	4.532	4.553	2.858	(90)	0.5×117.95	80

Table II. Lattice parameters of the different phases identified for the 420 nm-thick VO_2 film and determined by HRXRD.

VI. DISCUSSION

Orientations We propose two structural models in order to describe the in-plane epitaxial relationships of a $[010]_{M1}$-oriented VO_2 film grown on $Al_2O_3(0001)$. These models account for the observations made by Nag *et al.*,[27] where the two in-plane epitaxial growths are reported depending on the substrate temperature during the synthesis. The triplet signature reported by Fan *et al.*, and more recently by Théry *et al.*, now identifies the epitaxial relationship of the films as being *diagonal*.[22,55,56] However some results seem incompatible with these two models. In one instance, Zhao *et al.* reported triplets and doublets,[57] corresponding to a *diagonal* growth. But the angular differences between the satellites and the central peak of the triplets were found to be slightly different and explained by distinct angles along the vanadium "zig zag" chains. We believe that this observation could alternatively be due to the slight difference in Bragg angles between the central peak and the satellites. If not corrected, it induces a bias of $\delta\phi = \Delta\theta_B$ in the azimuthal angle ϕ of the central peak. In another instance, Fan *et al.* reported reflections with $(-2\varepsilon, 0, +2\varepsilon)$ triplet in agreement with the *diagonal* model.[55] However, one triplet reflection was indexed as $(002)_{M1}$, which should have appeared as a doublet according to the model. An explanation was given with a model consisting

of the simultaneous presence of the *on-axis* model with $[010]_R \parallel [10\bar{1}0]_{Al_2O_3}$ and the alternative *on-axis* model with $[001]_R \parallel [10\bar{1}0]_{Al_2O_3}$. However, this combination would give triplets at $(-\varepsilon, 0, +\varepsilon)$ positions, whereas only $(-2\varepsilon, 0, +2\varepsilon)$ triplets are reported. A combination of the *diagonal* and the *on-axis* models is also unlikely as quintuplets $(-2\varepsilon, -\varepsilon, 0, +\varepsilon, +2\varepsilon)$ and triplets $(-\varepsilon, 0, +\varepsilon)$ would have been expected. We do not have an explanation in this peculiar case. We shall only suggest a re-examination of the indexing of the reflection reported as $(002)_{M1}$, which did appear as a doublet in our measurements.

According to the multiplet structure we observed by diffraction, the present VO_2 film grew at high temperature according to the *diagonal* model. We established that the epitaxial bond is $[011]_R$ on $[21\bar{3}0]_{Al_2O_3}$ and that the rutile tetragonal c_R axis lies in the plane of the film (Fig. 1, top). This model is favored by the relatively small misfit between the atomic spacings along the considered directions: 2.747 Å for the Al-Al distance along the Al_2O_3 $[21\bar{3}0]$ direction and $5.376 = 2 \times 2.688$ Å for the V-V or O-O distance along the VO_2 $[011]$ direction. It corresponds to a 2.2% tensile stress for the film along this direction. The *on-axis* model would imply a higher strain along the substrate's $[100]$ direction, nearly 3.8%. Additionally, we found that the effect of the tensile strain on the whole film is very small for such a large thickness indicating a relaxation from the strain for the rutile-like *a* and *c* parameters. The out-of-plane strain we found is about -0.12%, which fits well with the thickness evolution of this strain reported by Théry *et al.*[22] The surface unit-cells of the three phases we identified are presented in Figure 9. The high temperature phase is not expected to be strictly tetragonal because of the strain, but it is not orthorhombic either for the in-plane angle between the two main axes is slightly less than 90°. Indeed, we can establish from the positions of the doublets that $[001]_R$ is about 2° off $[12\bar{3}0]_{Al_2O_3}$, whereas from the triplets, $[010]_R$ is about 1.9° off $[100]_{Al_2O_3}$, instead of 2.1° in the bulk tetragonal structure. The axes are thus slightly closer to the substrate directions, presumably because of the bonding epitaxial relationship along these axes.

Three-phase transition

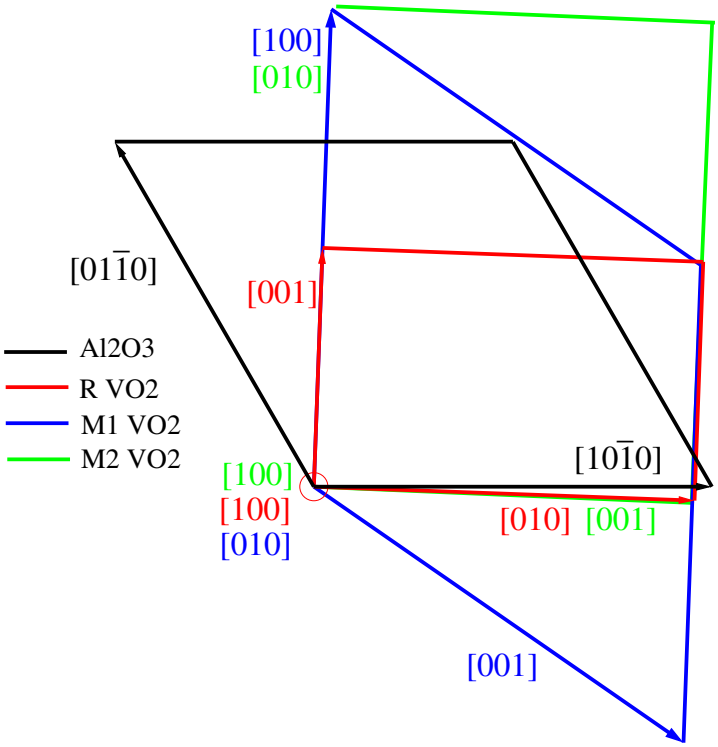

Figure 9. Representation of the surface unit-cells of the different VO_2 phases with respect to the one of the sapphire substrate (in black) in the case of the *diagonal* growth model. The monoclinic M1 phase is sketched in blue, with its [010] axis pointing out-of-plane. The monoclinic M2 phase appears in green and grows along the [100] direction. The tetragonal rutile R phase is in red, growing along the [100] direction.

The existence of a triple point in bulk VO_2 involving the most common polymorphs (M1, M2, and R) was recently reported by Park *et al.*[11] Our specular measurements indicate an insulator-to-metal transition that follows the sequence M1 $\Rightarrow$ M1 + M2 $\Rightarrow$ M2 + R, when heating the sample from RT up to 90°C. This observation seems in agreement with the VO_2 phase diagram versus uniaxial stress:[58] the M1 phase is expected to transform to the R phase via the M2 phase with temperature, when an uniaxial stress

along the c_R axis is imposed by the substrate.

An intermediary phase has already been reported by several groups for thin films near the MIT temperature. Théry *et al.* evidenced a third unidentified phase in an intermediate temperature range around the MIT for a VO_2 film grown by electron-beam evaporation on an Al_2O_3(0001) substrate kept at 500°C.[22] They closely followed the evolution of the specular reflection with temperature and observed that this phase has a larger lattice parameter along the growth direction. Considering the bulk lattice parameters (Table I), such an observation fits well with the presence of the M2 phase, as also suggested by our own measurements. Apart from the substrate nature, the stabilization of the M2 polymorph at high temperature seems to be also critically dependent on the synthesis method.[36,59] Okimura *et al.* showed that this intermediate insulating M2 phase is present only in the case of highly-oriented 200 nm-thick VO_2 films grown on Al_2O_3(0001) substrates by PLD or by reactive sputtering.[36] On the contrary, when the VO_2 films are grown on Si(100), the MIT proceeds directly from the insulating monoclinic M1 to the metallic tetragonal R phase. The films are polycrystalline on the Si substrate, whereas they turn out to be strained on Al_2O_3(0001). In this latter case, the M2 phase was detected over a wide range of temperature, even at room temperature where it competes with M1, with a small remaining contribution above the MIT temperature. The authors showed that it is still present, even at 104°C, when the films are synthesized by PLD, whereas it has almost totally disappeared at 73°C when the VO_2 films are grown by reactive sputtering. A seeding role of the interface is probable, which leads to the question of the interfacial region, where we believe the M2 phase is stabilised at high temperature. This hypothesis is supported by our complementary results from HRXRD and Raman spectroscopy. The existence of the intermediate M2 phase within a narrow range of temperature spanning from 65°C to 70°C is evidenced by Raman spectroscopy. Similarly, in-plane HRXRD also highlights a narrow range of temperature for the M2 phase existence. In contrast, out-of-plane HRXRD in specular configuration suggests that the M2 phase is still present at 90°C. A possible explanation

is that the M2 phase would be mainly present at the interface with the Al_2O_3 substrate, especially when the temperature increases. Out-of-plane HRXRD measurements in specular configuration probe the whole sample thickness, whatever the temperature and will therefore detect the M2 phase, even if it is restricted to the interfacial region. Due to a very shallow incidence angle, in-plane HRXRD probes a more limited region close to the sample surface. Regarding Raman spectroscopy, the detection of the Raman signal arising from the insulating M2 phase is hampered by the progressive appearance of the metallic R phase, above the MIT.

VII. CONCLUSION

The metal-insulator transition of a 420 nm-thick VO_2 film epitaxially strained on Al_2O_3(0001) was studied by combining the results from high-resolution X-ray diffraction and Raman spectroscopy. Three different VO_2 polymorphs are involved in the MIT: at room temperature, the film adopts the monoclinic M1 structure, while the high temperature phase is similar to the tetragonal rutile R polymorph. The third one corresponds to the monoclinic M2 phase, appearing close to the MIT temperature. The complementarity between Raman and XRD measurements is illustrated in the seemingly different temperature range of existence of the M2 polymorph, as the two techniques probe different depth scales. Raman spectroscopy evidences the intermediate M2 phase in a sharp temperature range spanning from 65 to 70 °C, whereas the depth-sensitivity of X-rays shows that this phase exists concomitantly with the R phase, well above the MIT temperature. This points more likely to an interfacial presence of the M2 phase, stressing the importance of precise and complementary structural investigations. Another keypoint of this work is to propose two structural models (designated as *on-axis* and *diagonal*) streamlining the in-plane epitaxial relationship observed in this particular case, but also in previous XRD works from literature. These models imply an in-plane tensile strain within the film (2 or 4% along the epitaxial direction). In the case of our film, the 2%

strain does not drastically affect the transition temperature, as it is found to be close to the one of bulk VO_2. In view of specific applications, strain engineering is known to be a powerful way for tailoring the transport and optical properties of VO_2, highly correlated to establishing the link between structure and macroscopic properties. In such a broader perspective, we believe that these models might help us understand the strain state of doped samples. A switch between the *diagonal* and the *on-axis* model could be expected to allow a better accommodation of the dopant within the VO_2 unit-cell, as the dopant concentration increases.

ACKNOWLEDGMENTS

The LANEF framework (ANR-10-LABX-51-01) is acknowledged for its support with mutualised infrastructure, as well as the Agence Nationale de la Recherche through the ANR-15-CE08-0035 *Smart_VOx* project.

REFERENCES

[1]F. J. Morin, Phys. Rev. Lett. **3**, 34 (1959).

[2]J. B. Goodenough, Journal of Solid State Chemistry **3**, 490 (1971).

[3]M. Gatti, F. Bruneval, V. Olevano, and L. Reining, Phys. Rev. Lett. **99**, 266402 (2007).

[4]Z. Yang, C. Ko, and S. Ramanathan, Annual Review of Materials Research **41**, 337 (2011), https://doi.org/10.1146/annurev-matsci-062910-100347.

[5]M. T. Nouman, J. H. Hwang, M. Faiyaz, K.-J. Lee, D.-Y. Noh, and J.-H. Jang, Opt. Express **26**, 12922 (2018).

[6]T. Driscoll, H.-T. Kim, B.-G. Chae, B.-J. Kim, Y.-W. Lee, N. M. Jokerst, S. Palit, D. R. Smith, M. Di Ventra, and D. N. Basov, Science **325**, 1518 (2009).

[7]S. Hormoz and S. Ramanathan, Solid-State Electronics **54**, 654 (2010).

[8]A. Hendaoui, N. Émond, S. Dorval, M. Chaker, and E. Haddad, Current Applied Physics **13**, 875 (2013).

[9]J. Zhou, Y. Gao, Z. Zhang, H. Luo, C. Cao, Z. Chen, L. Dai, and X. Liu, Scientific Reports **3**, 3029 (2017).

[10]M. Marezio, D. B. McWhan, J. P. Remeika, and P. D. Dernier, Phys. Rev. B **5**, 2541 (1972).

[11]J. H. Park, J. M. Coy, T. S. Kasirga, C. Huang, Z. Fei, S. Hunter, and D. H. Cobden, Nature **500**, 431 (2013), http://dx.doi.org/10.1038/nature12425.

[12]Y. Muraoka and Z. Hiroi, Applied Physics Letters **80**, 583 (2002).

[13]L. L. Fan, S. Chen, Z. L. Luo, Q. H. Liu, Y. F. Wu, L. Song, D. X. Ji, P. Wang, W. S. Chu, C. Gao, C. W. Zou, and Z. Y. Wu, Nano Letters **14**, 4036 (2014).

[14]J. Jeong, N. Aetukuri, T. Graf, T. D. Schladt, M. G. Samant, and S. S. P. Parkin, Science **339**, 1402 (2013).

[15]J. F. De Natale, P. J. Hood, and A. B. Harker, Journal of Applied Physics **66**, 5844 (1989).

[16]L. L. Fan, S. Chen, Y. F. Wu, F. H. Chen, W. S. Chu, X. Chen, C. W. Zou, and Z. Y. Wu, Applied Physics Letters **103**, 131914 (2013).

[17]Y. Cui and S. Ramanathan, Journal of Vacuum Science & Technology A **29**, 041502 (2011).

[18]C. H. Griffiths and H. K. Eastwood, Journal of Applied Physics **45**, 2201 (1974).

[19]J. Sakai, M. Zaghrioui, M. Matsushima, H. Funakubo, and K. Okimura, Journal of Applied Physics **116**, 123510 (2014).

[20]L. L. Fan, S. Chen, G. M. Liao, Y. L. Chen, H. Ren, and C. W. Zou, Journal of Physics: Condensed Matter **28**, 255002 (2016).

[21]V. Théry, A. Boulle, A. Crunteanu, and J. C. Orlianges, Applied Physics Letters **111**, 251902 (2017), https://doi.org/10.1063/1.5010147.

[22]V. Théry, A. Boulle, A. Crunteanu, J. C. Orlianges, A. Beaumont, R. Mayet, A. Mennai, F. Cosset, A. Bessaudou, and M. Fabert, Phys. Rev. B **93**, 184106 (2016).

[23]A. Tselev, I. A. Luk'yanchuk, I. N. Ivanov, J. D. Budai, J. Z. Tischler, E. Strelcov, A. Kolmakov, and S. V. Kalinin, Nano Letters **10**, 4409 (2010).

[24]Y. Oka, S. Sato, T. Yao, and N. Yamamoto, Journal of Solid State Chemistry **141**, 594 (1998).

[25]C. Leroux, G. Nihoul, and G. Van Tendeloo, Phys. Rev. B **57**, 5111 (1998).

[26]N. H. Azhan, K. Su, K. Okimura, M. Zaghrioui, and J. Sakai, Journal of Applied Physics **117**, 245314 (2015).

[27]J. Nag, E. Payzant, K. More, and R. Haglund Jr., Applied Physics Letters **98**, 251916 (2011).

[28]H. Le-Quoc, A. Lacoste, E. K. Hlil, A. Bès, T. Tan Vinh, D. Fruchart, and N. Skryabina, Journal of Alloys and Compounds **509**, 9906 (2011).

[29]J. M. Longo and P. Kierkegaard, P. Acta Chem. Scand. **24**, 420 (1970).

[30]J. Chamberland, J. Solid State Chem. **7**, 377 (1973).

[31]K. Rogers, Powder Diffr. **8**, 240 (1993).

[32]T. Huang, W. Parrish, N. Masciocchi, and P. Wang, Adv. X-Ray Anal. **33**, 295 (1990).

[33]S. Béchu, O. Maulat, Y. Arnal, D. Vempaire, A. Lacoste, and J. Pelletier, Surface and Coatings Technology **186**, 170 (2004), 7th International Workshop on Plasma-Based Ion Implantation.

[34]P. Vilanova-Martínez, J. Hernández-Velasco, A. Landa-Cánovas, and F. Agulló-Rueda, Journal of Alloys and Compounds **661**, 122 (2016).

[35]K. Okimura and J. Sakai, Japanese Journal of Applied Physics **48**, 045504 (2009).

[36]K. Okimura, J. Sakai, and S. Ramanathan, Journal of Applied Physics **107**, 063503 (2010).

[37]F. J. Wong, Y. Zhou, and S. Ramanathan, Journal of Crystal Growth **364**, 74 (2013).

[38]Z. P. Wu, S. Yamamoto, A. Miyashita, Z. J. Zhang, K. Narumi, and H. Naramoto, Journal of Physics: Condensed Matter **10**, L765 (1998).

[39]D. B. McWhan, M. Marezio, J. P. Remeika, and P. D. Dernier, Phys. Rev. B **10**, 490 (1974).

[40]P. Schilbe, Physica B: Condensed Matter **316-317**, 600 (2002), proceedings of the 10th International Conference on Phonon Scatte ring in Condensed Matter.

[41]P. Schilbe and D. Maurer, Materials Science and Engineering: A **370**, 449 (2004), 13th International Conference on Internal Friction and Ultrasonic Attenuation in Solids.

[42]J. Y. Chou, J. L. Lensch-Falk, E. R. Hemesath, and L. J. Lauhon, Journal of Applied Physics **105**, 034310 (2009).

[43]M. Zaghrioui, J. Sakai, N. H. Azhan, K. Su, and K. Okimura, Vibrational Spectroscopy **80**, 79 (2015).

[44]C. Marini, E. Arcangeletti, D. Di Castro, L. Baldassare, A. Perucchi, S. Lupi, L. Malavasi, L. Boeri, E. Pomjakushina, K. Conder, and P. Postorino, Phys. Rev. B **77**, 235111 (2008).

[45]J. M. Atkin, S. Berweger, E. K. Chavez, M. B. Raschke, J. Cao, W. Fan, and J. Wu, Phys. Rev. B **85**, 020101 (2012).

[46]S. Zhang, J. Y. Chou, and L. J. Lauhon, Nano Letters **9**, 4527 (2009).

[47]A. C. Jones, S. Berweger, J. Wei, D. Cobden, and M. B. Raschke, Nano Letters **10**, 1574 (2010).

[48]E. Strelcov, A. Tselev, I. Ivanov, J. D. Budai, J. Zhang, J. Z. Tischler, I. Kravchenko, S. V. Kalinin, and A. Kolmakov, Nano Letters **12**, 6198 (2012).

[49]K. Okimura, N. Hanis Azhan, T. Hajiri, S.-i. Kimura, M. Zaghrioui, and J. Sakai, Journal of Applied Physics **115**, 153501 (2014).

[50]R. Srivastava and L. L. Chase, Phys. Rev. Lett. **27**, 727 (1971).

[51]G. I. Petrov, V. V. Yakovlev, and J. Squier, Applied Physics Letters **81**, 1023 (2002).

[52]S.-J. Chang, W.-K. Hong, H. J. Kim, J. B. Lee, J. Yoon, H. C. Ko, and Y. S. Huh, Nanotechnology **24**, 345701 (2013).

[53]H. Kim, T. V. Slusar, D. Wulferding, I. Yang, J.-C. Cho, M. Lee, H. C. Choi, Y. H. Jeong, H.-T. Kim, and J. Kim, Applied Physics Letters **109**, 233104 (2016).

[54]M.-W. Kim, S.-S. Ha, O. Seo, D. Y. Noh, and B.-J. Kim, Nano Letters **16**, 4074 (2016).

[55]L. L. Fan, Y. F. Wu, C. Si, G. Q. Pan, C. W. Zou, and Z. Y. Wu, Applied Physics Letters **102**, 011604 (2013), https://doi.org/10.1063/1.4775580.

[56]V. Théry, A. Boulle, A. Crunteanu, J. C. Orlianges, A. Beaumont, R. Mayet, A. Mennai, F. Cosset, A. Bessaudou, and M. Fabert, Journal of Applied Physics **121**, 055303 (2017), https://doi.org/10.1063/1.4975117.

[57]Y. Zhao, J. H. Lee, Y. Zhu, M. Nazari, C. Chen, H. Wang, A. Bernussi, M. Holtz, and Z. Fan, Journal of Applied Physics **111**, 053533 (2012), https://doi.org/10.1063/1.3692391.

[58]J. Cao, Y. Gu, W. Fan, L. Q. Chen, D. F. Ogletree, K. Chen, N. Tamura, M. Kunz, C. Barrett, J. Seidel, and J. Wu, Nano Letters **10**, 2667 (2010).

[59]K. Okimura, T. Watanabe, and J. Sakai, Journal of Applied Physics **111**, 073514 (2012).